Early-Stage Dynamics of Light-Matter Interaction Leading to the Insulator-to-Metal Transition in a Charge Ordered Organic Crystal

Y. Kawakami,[1] T. Fukatsu,[1] Y. Sakurai,[1] H. Unno,[1] H. Itoh,[1,2] S. Iwai,[1,2,*] T. Sasaki,[2,3] K. Yamamoto,[4] K. Yakushi,[4] and K. Yonemitsu[4]

[1]*Department of Physics, Tohoku University, Sendai 980-8578, Japan*
[2]*JST, CREST, Sendai 980-8578, Japan*
[3]*Institute for Materials Research, Tohoku University, Sendai 980-8577, Japan*
[4]*Institute for Molecular Science, Okazaki 444-8585, Japan*

(Received 23 May 2010; published 7 December 2010)

Ultrafast dynamics of the light-matter interaction in a charge-ordered molecular insulator α-(BEDT-TTF)$_2I_3$ were studied by pump-probe spectroscopy using few-optical-cycle infrared pulses (pulse width 12 fs). Coherent oscillation of the correlated electrons and subsequent Fano destructive interference with intramolecular vibration were observed in time domain; the results indicated a crucial role for electron-electron interplay in the light-matter interaction leading to the photoinduced insulator-to-metal transition. The qualitative features of this correlated electron motion were reproduced by calculations based on exact many-electron-phonon wave functions.

DOI: 10.1103/PhysRevLett.105.246402 PACS numbers: 78.47.J−, 71.30.+h, 78.55.Kz

The interaction between light and matter strongly depends on the type of the material system. For semiconductors and their nanostructures, coherent electron-phonon (e-ph) interactions govern the formation of quasiparticles such as polarons immediately after electronic excitation by an ultrashort pulse [1–4]. However, in charge-ordered (CO) insulators formed by Coulomb repulsion [electron-electron (e-e)] interaction, photoexcitation can sometimes produce more dramatic changes in the dielectric or conduction properties, e.g., the photoinduced melting of charge order or, equivalently, the photoinduced insulator-to-metal transition (PIMT) [5,6]. Thus, practical optical manipulation of the material phase of a CO system will first require a clear understanding of the correlated electron motion involved. However, such correlated electron dynamics immediately after the photoexcitation remain hidden, because the time resolution is not sufficiently high to detect an excited electron motion before it is significantly affected by the phonon motion.

In organic molecular solids with strong electron correlation, a CO gap (Δ_{CO}) of 0.1–0.2 eV reflects the intermolecular charge transfer (CT) excitation energy of the correlated electrons. The time scale of the correlated electron motion is $\sim\hbar/\Delta_{CO} = 20$–$40$ fs. This allows the electron motions to be directly detected via measurements with a time resolution of 10 fs. A typical example of such a material is the layered organic salt α-(BEDT-TTF)$_2I_3$ (BEDT-TTF: bis(ethylenedithio)-tetrathiafulvalene), which exhibits a charge order below the metal [Fig. 1(b)]-CO insulator [Fig. 1(a)] transition temperature (T_{CO}) of 135 K [7–13]. The metal-CO insulator transition in this compound can be regarded as a Wigner-like electronic transition [7–9]. Photoexcitation of the CO insulator causes an efficient (50–100 molecules/photon) and ultrafast (< 200 fs) insulator-to-metal transition that can actually be observed using midinfrared and terahertz spectroscopy at time resolutions of 200 fs to 1 ps [11,12]. Nevertheless, thus far, no study has reported the successful observation of correlated electron motion in the light-matter interaction leading to the PIMT.

In the present study, we employed few-optical-cycle infrared pulses (pulse width, $\sim$12 fs) in the pump-probe measurement to investigate the early-stage dynamics of electron motion in α-(BEDT-TTF)$_2I_3$. The observations of the coherent electron oscillation and the Fano interference with the intramolecular C=C stretching vibration provided a clear picture of the light-matter interaction in the primary process of the PIMT.

Single crystals of α-(BEDT-TTF)$_2I_3$ ($2 \times 1 \times 0.1$ mm) were prepared by using a method described in the

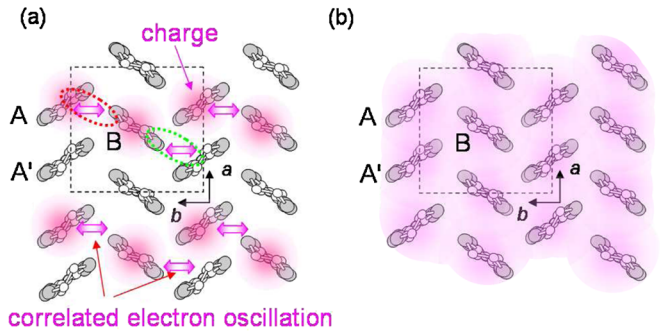

FIG. 1 (color online). Schematic representation of molecular arrangement in the (a) low-temperature CO phase and (b) metallic phase. Clouds and arrows in (a) indicate the charge distribution and the electron oscillation, respectively. Dashed circles represent the b_2' (between A and B sites) bond and b_2 (between B and A' sites) bond, respectively.

literature [7]. Reflection-detected pump-probe measurements were performed using a Ti:Al_2O_3 amplifier with two-stage degenerate optical parametric amplifiers (OPAs) [14] in order to generate a broadband (0.65–1 eV) spectrum. This broadband infrared pulse was compressed using an active-mirror (Flexible Optical, MMDM 11 × 39 mm) compressor [14]. The pulse width was estimated to be 12 fs, which corresponds to three optical cycles, using a second harmonic generation frequency-resolved optical gating technique. The time resolution at the sample position was 15 fs as an FWHM of the cross-correlation between the pump and the probe pulses.

Figure 2(a) shows the optical conductivity (σ) spectrum along the $//b$ axis at 10 K (CO) and 150 K (metallic). The σ spectrum at 10 K exhibits an intermolecular CO gap in energy regions of ~0.1 eV indicating the CT excitation of the correlated electron motion [15]. Figure 2(b) shows the photo-induced reflectivity change [$\Delta R/R = (R' - R)/R$, where R and R' represent the reflectivity before and after the excitation, respectively], which was measured by pump-probe spectroscopy at a time resolution of ~200 fs (pump: 0.89 eV; excitation intensity, I_{ex}: 0.1 mJ cm^{-2}; a pump-probe delay time $t_d = 100$ fs) along the $//b$ axis at 20 K [11]. As seen in Fig. 2(b), the $\Delta R/R$ spectrum is analogous to the spectral difference $[R(150\text{ K}) - R(10\text{ K})]/R(10\text{ K})$ [solid curve (× 0.5)], indicating that a metallic state is generated by the photoexcitation using the ~150 fs pulse. The spectral range of the pump and the probe pulses generated by the degenerate OPA [indicated by the shaded area in Fig. 2(a)] corresponds to the high-energy side of the intermolecular CT transition. The $\Delta R/R$ spectrum shows a marked decrease at ~0.7 eV, which indicates the occurrence of the PIMT.

Figure 2(c) shows the time evolution of $\Delta R/R$ measured at 0.7 eV at 20 K ($I_{ex} = I_0$, 0.05 I_0, where $I_0 = 0.03$ mJ cm^{-2}) and 80 K ($I_{ex} = I_0$) under the excitation by 12 fs pulses, reflecting the generation dynamics of the photoinduced metallic state. The I_{ex} value for $I_0 = 0.03$ mJ/cm^2 corresponds to a density of 1 photon/1500 molecules for the 0.89 eV excitation. The time scale of the initial rise in the $\Delta R/R$ signal (< 20 fs) is as fast as that of the correlated electron motion, as discussed later.

The high-frequency oscillating component of $\Delta R/R$ (20 K, $I_{ex} = I_0$) was obtained by using a Fourier high-pass (> 300 cm^{-1}) filter [Fig. 3(a)]. In addition, a time-frequency spectrogram [Fig. 3(b)] and time-resolved spectra [Figs. 4(b)–4(e)] were obtained by wavelet (WL) analysis of the oscillating component. As indicated by the black dashed circle denoted as (i) in Figs. 3(a) and 3(b), the spectrogram is dominated by the broad signal at ~1800 cm^{-1} for $t_d < 50$ fs. The signal peak exhibits a drastic frequency change with t_d between (ii) ~1000 cm^{-1} and (iii) 1450 cm^{-1} for $t_d = 50$–200 fs. Then, the (iv) signal approaches ~820 cm^{-1} for $t_d > 200$ fs.

It is noteworthy that the broad spectrum at ~1800 cm^{-1} exhibiting the spectral gap at ~1000 cm^{-1} for $t_d = 30$ fs [Fig. 4(b) and (i) in Figs. 3(a) and 3(b)] is analogous to the

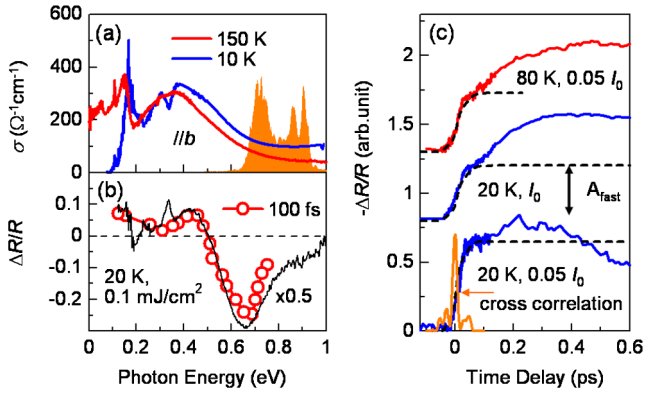

FIG. 2 (color online). (a) σ spectrum along the $//b$ axis at 10 K (CO phase) and 150 K (metallic phase). The spectral range of the pump and the probe 12 fs pulse is indicated by the shaded area. (b) $\Delta R/R$ spectrum at $t_d = 100$ fs measured by pump-probe spectroscopy at a time resolution of ~200 fs [11]. The spectral difference $[R(150\text{ K})\text{-}R(10\text{ K})]/R(10\text{ K})$ is represented by the solid curve (× 0.5). (c) Time evolutions of $\Delta R/R$ measured at 0.7 eV at 20 K ($I_{ex} = 0.05 I_0$ and I_0), and 80 K ($I_{ex} = I_0$). The cross correlation profile between the pump and probe pulses is indicated as a response function [$G(t)$].

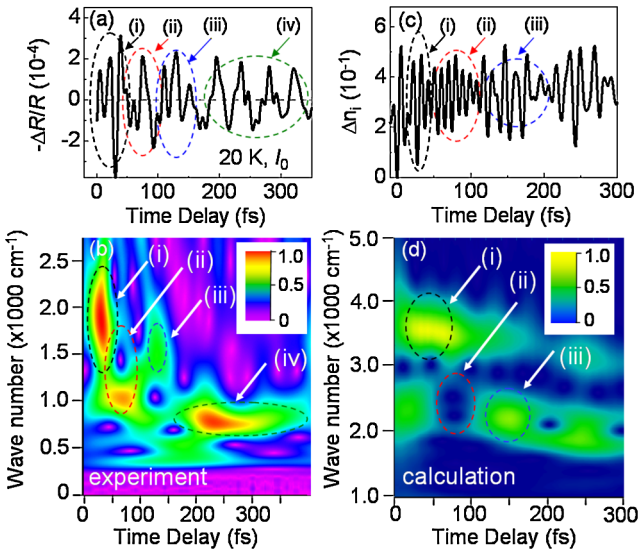

FIG. 3 (color online). (a) High-frequency oscillating component of $\Delta R/R$ at 20 K for $I = I_0$, which was obtained by using a Fourier high-pass (> 300 cm^{-1}) filter. (b) Time-frequency spectrogram was calculated by wavelet analysis of the high-frequency oscillating component. (c) Calculated photoinduced charge-density modulation (Δn_i) at molecule A in the extended Peierls-Hubbard model with EMV coupling (see text). (d) Spectrogram of calculated Δn_i.

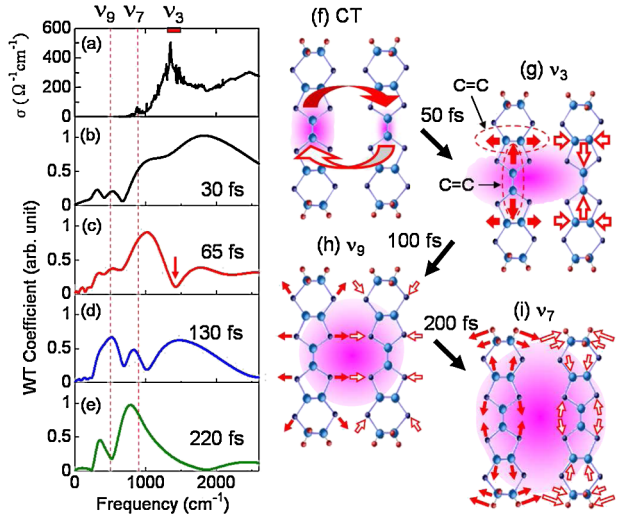

FIG. 4 (color online). (a) Optical conductivity spectrum measured at 10 K. (b)–(e) Time-resolved spectra calculated from Fig. 3(a). (f)–(i) Schematic illustration of (f) intermolecular electron modulation and intramolecular vibrations (g) ν_3, (h) ν_9, and (i) ν_7.

steady state optical conductivity spectrum [Fig. 4(a)]. Therefore, the oscillation at 1800 cm^{-1} is attributable to the electron oscillation reflecting the CO gap. This is the first observation of electron oscillation in the time domain. Such intermolecular electron oscillation is efficiently induced between the charge-rich sites (A and B sites) through the b_2' bond (upper dashed circle) and between the charge-rich site and charge-poor site (B and A' sites) through the b_2 bond (lower dashed circle) [9,16,17], as illustrated by the arrows in Figs. 1(a) and 4(f).

Considering that C═C stretching modes ν_3 [shown in Fig. 4(g)] appear between 1352 and 1476 cm^{-1} [15,18], the spectral hollow that appears at ~1450 cm^{-1} [arrow in Fig. 4(c) and (ii) in Figs. 3(a) and 3(b)] is attributable to the destructive interference [3] between the electron oscillation and the intramolecular ν_3 mode. The observation of such destructive interference which is attributable to Fano antiresonance [19] at ~50 fs indicates that the electron oscillation begins to interact coherently with the intramolecular ν_3 mode at the finite time delay.

Taking into account the strong electron molecular vibration (EMV) coupling of the ν_3 mode [18], it is reasonable to consider that the electron oscillation selectively induces the intermolecular antiphase ν_3 vibration, as shown in Figs. 4(f) and 4(g) [18]. After 100 fs, the hollow at ~1450 cm^{-1} disappears and a broad band appears at 1450 cm^{-1}, reflecting the electronic dephasing [Fig. 4(d) and (iii) in Fig. 3(b)]. Then, the disappearance of the broad 1450 cm^{-1} mode indicates that the coherent ν_3 vibration is dephased by interaction with other vibrations.

The other signals at ~500 cm^{-1} [Fig. 4(d)] and 820 cm^{-1} [Fig. 4(e)] after $t_d = 150$ fs are, respectively, attributable to the ν_9 (508 cm^{-1}) (called breathing mode) and ν_7 (896 cm^{-1}) modes, as illustrated in Figs. 4(h) and 4(i) [18]. These modes also show large EMV coupling constants (ν_3: 0.746; ν_9: 0.476; ν_7: 0.117, in dimensionless units). Figures 3(b) and 4(c)–4(e) suggest that sequential changes occurred in the interacting modes from the local C═C stretching mode (ν_3) to the more delocalized breathing mode (ν_9) and ν_7 mode showing the pathway of e-e and e-ph interactions that leads to the insulator-to-metal transition from the electron oscillation.

To consider the correlated electron motion and the coherent interplay between the electron and intramolecular ν_3 vibration, we calculated the photoinduced electron dynamics by numerically solving the time-dependent Schrödinger equation for the exact many-body wave function for electrons coupled with classical intermolecular phonons and quantum intramolecular phonons. Here, we add the EMV coupling to the extended Peierls-Hubbard model described in Ref. [16]

$$H = \sum_{\langle ij\sigma\rangle}[(t_{i,j} \pm \alpha_{i,j}u_{i,j})c^{+}_{i\sigma}c_{j\sigma} + \text{H.c.}] + U\sum_i n_{i\uparrow}n_{i\downarrow} + \sum_{\langle ij\rangle} V_{i,j}n_i n_j + \sum_{\langle ij\rangle}(K_{i,j}/2)u^2_{i,j} + \sum_{\langle ij\rangle}(K_{i,j}/2\omega^2_{i,j})\dot{u}^2_{i,j} + g\sum_i (b_i + b_i^{+})(n_i - 3/2) + \omega_b\sum_i b_i^{+}b_i$$

where $c^{+}_{i\sigma}$ creates an electron with spin σ at site i, $n_{i\sigma} = c^{+}_{i\sigma}c_{i\sigma}$, $n_i = \sum_\sigma n_{i\sigma}$, $u_{i,j}$ denotes the intermolecular phonon's displacement, b_i^{+} creates a quantum phonon of energy ω_b, and g is the EMV coupling strength. The other notations are standard and are introduced in Ref. [16]. Using an eight-site periodic cluster and the same model parameters as those reported in Ref. [16] ($\omega_b = 0.36$ eV, $g = 0.0625$ eV, and an oscillating electric field along the b axis having a Gaussian profile of duration 5 fs and center frequency $\omega_{\text{ext}} = 0.35$ eV), we calculated the time evolution of n_i at molecule A [Fig. 1(a)] for $t_d < 300$ fs [Fig. 3(c)] and carried out WL analysis [Fig. 3(d)]. The broad peak from 3000 to 4000 cm^{-1} at around $t_d = 30$ fs corresponds to that of the calculated conductivity spectrum in Ref. [16], indicating that the peak is attributable to the electron oscillation shown in Fig. 1(a) [(i) in Figs. 3(c) and 3(d)]. The difference between the experimental and calculated values of the conductivity peak (experiment; 1000–2000 cm^{-1}, calculation; 3000–4000 cm^{-1}) can be attributed to the small cluster size. We actually demonstrated that the conductivity peak increases as the cluster size decreases; i.e., the peak energy is 0.3 eV for 12 sites [16] and 0.2 eV for 144 sites [17], respectively. For $t_d =$ 50–100 fs, the spectral hollow at 2000–3000 cm^{-1} is attributable to the destructive interference between the correlated electron oscillation and the phonon [(ii) in Figs. 3(c) and 3(d)]. Then, the phonon peak appears after $t_d = 100$ fs [(iii) in Figs. 3(c) and 3(d)]. This calculated WL spectrogram that reflects the electron-ν_3 vibration

interference is qualitatively analogous to the experimental result [Fig. 3(b)]. For $t_d > 100$ fs, however, the observed WL spectrogram cannot be reproduced by the calculated one because the other vibrations are not taken into account in the calculation. More detailed comparisons between the experimental and the calculated results have been reported for the reaction dynamics in few-body atomic or molecular systems [20]. However, such close discussion might be difficult for CO systems because they have many degrees of freedom and very few theoretical studies have been conducted on the dynamics of the CO systems [16,17].

As indicated by the dashed curve in Fig. 2(c), the time required for the generation of the metallic state (τ_r) is evaluated as 15 fs at 20 K for $I_{ex} = 0.05I_0$ using the equation $\Delta R(t)/R = \int_{-\infty}^{+\infty} A_{fast}[1 - \exp(-t/\tau_r)]G(t - t')dt'$, where A_{fast} and $G(t)$ are the coefficient and response function, respectively. Here, the cross-correlation profile between the pump and the probe pulses was used as $G(t)$ in Fig. 2(c). A τ_r value of 15 fs is comparable to the time scale of the electron oscillation (1800 cm^{-1}) in Fig. 3(a), indicating that the early-stage dynamics of the PIMT are driven by the electronic response. This fast generation process dominates for the weak excitation ($I_{ex} = 0.05I_0$) at 20 K. However, the contribution of an additional slower ($\sim$ 300 fs) growth component increases with I_{ex} and temperature, as indicated by the result for the strong excitation ($I_{ex} = I_0$) at 20 K and at high temperature 80 K for $I_{ex} = 0.05I_0$, as shown in Fig. 2(c), reflecting the generation of the quasistable metallic state [11,12]. Considering that the coherent intramolecular vibrations are detected during this slower ($\sim$ 300 fs) growth, it is inferred that the quasistable metallic state is generated by the interplay between the electron oscillation and the vibrations.

The above results provide a clear microscopic view of the light-electron-lattice interactions leading up to the PIMT. It should be noted that this view is markedly different from the traditional description of the e-ph interactions in the framework of thermodynamic analysis such as that using a two-temperature model [4]; i.e., the e-ph interaction begins to start before the electrons reach the quasi equilibrium state.

In summary, we observed the coherent oscillation of correlated electrons and Fano destructive interference with intramolecular vibrations in the early-stage dynamics of the PIMT in the CO organic salt α-(BEDT-TTF)$_2I_3$ by pump-probe spectroscopy using few-optical-cycle infrared pulses.

We would like to thank M. Saito (Tohoku University) for technical support. This work was supported by a Grant-in-Aid for Scientific Research on Innovation Areas (New Frontier in Materals Research by Molecular Degrees of Freedom, 20110005).

*s-iwai@m.tohoku.ac.jp

[1] J. Shah, *Ultrafast Spectroscopy of Semiconductors and Semiconductor Nanostructures* (Springer, Berlin, 1999), 2nd ed.
[2] Y. Toyozawa, *Optical Process in Solids* (Cambridge, U.K., 2003).
[3] M. Hase, M. Kitajima, A. M. Constantinescu, and H. Petek, Nature (London) **426**, 51 (2003).
[4] R. D. Averitt and A. J. Taylor, J. Phys. Condens. Matter **14**, R1357 (2002).
[5] Special issue on Photo-Induced Phase Transitions and Their Dynamics, edited by M. Gonokami and S. Koshihara [J. Phys. Soc. Jpn. **75**, 011001 (2006)].
[6] K. Yonemitsu and K. Nasu, Phys. Rep. **465**, 1 (2008).
[7] K. Bender, I. Henning, D. Schweitzer, K. Dietz, H. Endres, and H. J. Keller, Mol. Cryst. Liq. Cryst. **108**, 359 (1984).
[8] M. Dressel, G. Gruner, J. P. Poget, A. Breining, and D. Schweitzer, J. Phys. I (France) **4**, 579 (1994).
[9] T. Kakiuchi, Y. Wakabayashi, H. Sawa, T. Takahashi, and T. Nakamura, J. Phys. Soc. Jpn. **76**, 113702 (2007).
[10] N. Tajima, J. Fujisawa, N. Naka, T. Ishihara, R. Kato, Y. Nishio, and K. Kajita, J. Phys. Soc. Jpn. **74**, 511 (2005).
[11] S. Iwai, K. Yamamoto, A. Kashiwazaki, F. Hiramatsu, H. Nakaya, Y. Kawakami, K. Yakushi, H. Okamoto, H. Mori, and Y. Nishio, Phys. Rev. Lett. **98**, 097402 (2007).
[12] H. Nakaya, K. Itoh, Y. Takahashi, H. Itoh, S. Iwai, S. Saito, K. Yamamoto, and K. Yakushi, Phys. Rev. B **81**, 155111 (2010).
[13] H. Seo, J. Merino, H. Yoshioka, and M. Ogata, J. Phys. Soc. Jpn. **75**, 051009 (2006).
[14] D. Brida, G. Cirmi, C. Manzoni, S. Bonora, P. Villoresi, S. De Silvestri, and G. Cerullo, Opt. Lett. **33**, 741 (2008).
[15] Y. Yue, K. Yamamoto, M. Uruichi, C. Nakano, K. Yakushi, S. Yamada, T. Hiejima, and A. Kawamoto, Phys. Rev. B **82**, 075134 (2010).
[16] S. Miyashita, Y. Tanaka, S. Iwai, and K. Yonemitsu, J. Phys. Soc. Jpn. **79**, 034708 (2010).
[17] Y. Tanaka and K. Yonemitsu, J. Phys. Soc. Jpn. **79**, 024712 (2010).
[18] M. E. Kozlov, K. I. Pokhodina, and A. A. Yurchenko, Spectrochim. Acta, Part A **45**, 437 (1989).
[19] D. Neuhauser, T. J. Park, and J. I. Zink, Phys. Rev. Lett. **85**, 5304 (2000).
[20] S. A. Rice and M. Zhao, *Optical Control of Molecular Dynamics* (Wiley-Interscience, New York, 2003).